Int J Comput Vis
DOI 10.1007/s11263-016-0919-0

Automatic Sleep System Recommendation by Multi-modal RBG-Depth-Pressure Anthropometric Analysis

Cristina Palmero[1] · Jordi Esquirol[2] · Vanessa Bayo[2] · Miquel Àngel Cos[2] · Pouya Ahmadmonfared[1] · Joan Salabert[3] · David Sánchez[3] · Sergio Escalera[1,4]

Received: 15 August 2015 / Accepted: 26 May 2016

Abstract This paper presents a novel system for automatic sleep system recommendation using RGB, depth and pressure information. It consists of a validated clinical knowledge-based model that, along with a set of prescription variables extracted automatically, obtains a personalized bed design recommendation. The automatic process starts by performing multi-part human body RGB-D segmentation combining GrabCut, 3D Shape Context descriptor and Thin Plate Splines, to then extract a set of anthropometric landmark points by applying orthogonal plates to the segmented human body. The extracted variables are introduced to the computerized clinical model to calculate body circumferences, weight, morphotype and Body Mass Index categorization. Furthermore, pressure image analysis is performed to extract pressure values and at-risk points, which are also introduced to the model to eventually obtain the final prescription of mattress, topper, and pillow. We validate the complete system in a set of 200 subjects, showing accurate category classification and high correlation results with respect to manual measures.

Keywords Sleep system recommendation · RGB-Depth data · Pressure imaging · Anthropometric landmark extraction · Multi-part human body segmentation

Communicated by Hiroshi Ishikawa, Takeshi Masuda, Yasuyo Kita and Katsushi Ikeuchi.

✉ Cristina Palmero
c.palmero.cantarino@gmail.com

Jordi Esquirol
jordi.esquirol@eug.es

Vanessa Bayo
vanesa.bayo@eug.es

Miquel Àngel Cos
mcos@car.edu

Pouya Ahmadmonfared
pouyaam@gmail.com

Joan Salabert
joansalabert@dormity.com

David Sánchez
davidsanchez@dormity.com

Sergio Escalera
sergio@maia.ub.es

[1] Computer Vision Center, Campus UAB, Edifici O, 08193 Cerdanyola del Vallès, Barcelona, Spain

[2] Servei Universitari de Recerca en Fisioteràpia (S.U.R.F), Escola Universitària Gimbernat, Avinguda de la Generalitat, 202-206, 08174 Sant Cugat del Vallès, Barcelona, Spain

[3] Dormity.com®, Via Augusta, 85-87, 08174 Sant Cugat del Vallès, Barcelona, Spain

[4] Dept. Matemàtica Aplicada i Anàlisi, UB, Gran Via de les Corts Catalanes 585, 08007 Barcelona, Spain

1 Introduction

Sleep health is one of the most important health aspects of the modern society. A poor sleep quality can lead to physical and psychological problems. Sleep ergonomics have recently become specially crucial, being the sleep environment a key mechanism for a correct sleep initiation quality and preservation during the night. Particularly the mattress, as a design product which has to adapt itself to the dimensional limitations of the human body, must present specific ergonomic features that ease the user's sleep in the proper postures, adapting to the different morphological types of the human body. The scientific literature includes a number of works focusing on human bodies categorization depending on their morphological type, some of them dealing with the modeling of mattresses (Matsuo et al. 2011) and cervical pillows pre-

Published online: 21 June 2016

scription (Gordon and Grimmer-Somers 2011; Gordon et al. 2010, 2009; Zuberi et al. 2004; Kim et al. 2013; Wong et al. 2013; Lazzaro et al. 2014), and with the sleep ergonomics analysis (Verhaert et al. 2011c; DeVocht et al. 2006), eventually defining the *sleep system* concept (Verhaert et al. 2011b).

Scientific evidence has determined that the mattresses comfort perception and their mechanical properties analyzed subjectively by users—mainly the elderly—is not sufficiently precise as to recommend customers to simply choose their future mattress through test in store (López-Torres et al. 2008); a predictive model could probably facilitate the sleep system choice with a greater scientific basis.

The analysis of scientific literature highlights the importance of the mattress-pillow combination characteristics (Sáenz et al. 2011) for a healthy rest (Leilnahari et al. 2011) and gives rise to a possible conceptualization of morphotypical intervals and morphological criteria, and the user's interval determination and categorization from his body measures. Such measures can be obtained through anthropometric analysis, which measures distances and circumferences between landmark points of the body. However, the use of geometrical instruments or markers to obtain them is a time consuming and obtrusive practice that may not be appropriate in a store setting.

In addition to anthropometric analysis, the study of the pressure distribution exerted by a person resting on a mattress surface is also fundamental, and hence the need for its presence in an individualized model of sleep system prescription. Such study is considered a preventive measure of pressure sores, accepted in emergency services and in situations where the patient mobility remains diminished (Miller et al. 2013).

The clinical goal of this work is the design, implementation and validation of a computerized model that recommends a sleep system—mattress, topper and pillow combination—that best suits customers' individual needs. To do so, we combine a mathematical model from the scientific clinical literature and automatic 2D and 3D imaging methods that allow to calculate distances and body geometries which are useful for morphotype analysis. To the best of our knowledge, this represents the first state-of-the-art computer vision system that automatically recommends the sleep system, performing feature extraction and fusion from pressure maps, 2D, and 3D images, and obtaining final recommendation based on computerized clinical knowledge.

1.1 Related Work

The experience on analysis of anthropometric measures through automatic imaging methods is long (Nechala et al. 1999). Fixed whole body 3D laser range scanners have been widely used for this purpose since they obtain an accurate scan of the body, but at the expense of an extensive post-processing and expensive equipment. An example of work that uses this type of acquisition device is the proposal of Allen et al. (2004), who used whole-body scans to learn how body shape varies between individuals in all parts of the body to morph a complete digital human body model—combination of surface model and inner skeleton—. However, the anthropometric landmarks were located by placing markers on the human body prior to scanning. Azouz et al. (2006) tackled this issue by learning landmark characteristics and their spatial relationships from a set of human scans were the landmarks were identified, and modeled such relationships as a Markov Random Field. More recently, the release of low-price multi-sensor devices such as Microsoft Kinect® based on structured light technology, which are also portable and compact enough to be easily installed in any environment, has greatly facilitated the task of non-invasive human body measurement (Clarkson et al. 2014; Espitia-Contreras et al. 2014). The Kinect system is capable of capturing visual RGB-depth (RGB-D) information and generate real-time depth maps containing discrete range measurements of the physical scene, which can be later re-projected as a set of discrete 3D points. Such depth map generation method has been analyzed by several research groups to determine and tackle its limitations (Martinez and Stiefelhagen 2014). In spite of such limitations, Kinect has been used in a wide spectrum of applications that require the automatic extraction of anthropometric or soft biometric measures, e.g. in clothing (Wang et al. 2014; Uhm et al. 2015), person re-identification (Lorenzo-Navarro et al. 2013; Mogelmose et al. 2013), face recognition (Gupta et al. 2010), rehabilitation (Reyes et al. 2013; Cippitelli et al. 2015), and workplace ergonomics (Huang and Pan 2014). Nguyen et al. (2014) recently proposed a novel method to estimate human weight, height and gender. Most of the aforementioned works rely on the human body segmentation and skeleton extraction methods provided by Microsoft SDK. However, this is not applicable when the person is lying on a mattress. Several techniques have been described to find body parts and compute body measures without such prior. An example is the work of Madadi et al. (2015), who proposed a model based system where body part labels of the points in the 3D point cloud are computed from a defined model after 3D alignment using Shape Context descriptors and Support Vector Machines (SVM). In the context of sleep monitoring, Yu et al. (2012) proposed a system to automatically detect sleep position, movement and breathing using depth-based information from Kinect. They placed the camera over the subject, behind the head of the subject, suspending from the ceiling. Assuming that the head was always higher than the pillow surface, they performed subject's torso and head detection with the following approach: first, they generated cross-sections from the shallowest point of the depth image to the depth of the bed; then, they extracted components from each

cross-section applying connected component analysis; for head detection, they looked for sphere candidates throughout the extracted components, leveraging on motion information from the video sequences; finally, to obtain torso location they searched cuboid candidates instead. More recently, Yang et al. (2014) presented a different sleep monitoring system based on a graph-based event classification scheme to detect episodes of abnormal breathing. They re-projected depth pixels to a virtual viewpoint image, where the virtual camera was located parallel to the sleeping subject, and classified observations into two cross-sections that correspond to the subject's chest and abdomen, each modeled by an ellipse.

On another front, sensitive-pressure bedsheets have been extensively used for monitoring sleep postures in clinical settings. Pressure image analysis can be challenging due to lack of informative shape information produced by self-occlusions, low-resolution and incomplete body pressure maps—some limbs may be missing if the pressure exerted is not high enough. As with 3D camera devices, digital human models have also been applied to pressure maps (Harada et al. 1999, 2001), which are able to estimate the position of the different body parts. Yousefi et al. (2011) used a 2D parametric model to detect areas of the body which are at risk of developing a pressure ulcer. However, most of the works rely on pressure signal features combined with classifiers such as SVM or k-Nearest Neighbors (kNN) for posture recognition (Foubert 2010), or spatial and geometrical features based on a grid division of the pressure map combined with Hidden Markov Models (HMM) for continuous posture evaluation (Liu et al. 2013, 2014).

Multi-modal strategies have gained more attention lately to enrich data representation, offsetting the weaknesses of one modality by the strengths of the other. In our context, few works have combined pressure sensors with other image acquisition devices, most of them for posture recognition purposes (Huang et al. 2010). In particular, Metsis et al. (2014) fused temporally-synchronized pressure maps and depth data from Kinect for sleep monitoring, using template matching, kNN and SVM for posture recognition and HMM for motion classification.

Currently, some of the most used methods for automatic anthropometric analysis in the context of personalized bed design have used plain measures estimated automatically from cameras or scanners. One of them is Ikélo® from Custom8®, an optical measurement system which outputs 2D body contours from both sagittal and frontal planes, such as height, breadth, and depth, at shoulder, breast, waist, pelvis, and hip. It also measures body weight and gives an estimate of the partial weights of body segments. It includes an expert module that recommends the best sleep system for the user based on the aforementioned measures. To do so, the subject has to stand up in front of the system in both poses, which may be a demerit in the context of a store setting, where a quick and user friendly service is crucial. However, since silhouette extraction of body contours provides no information on body circumferences, manual measurements of body circumferences must be performed if needed. Other applications are based on pressure information. Dynasleep®, created by the same company, is an active sleep system equipped with integrated indentation sensors that estimates the spine position during sleep so as to dynamically adjust the mattress. Both are used in the work of Verhaert et al. (2011a), which fuses the information of both sensors and creates a complete digital human model based on consecutive superelliptic cross-sections in order to assess spine support on a bedding system while the subject is sleeping. Since body circumferences could not be provided by Ikélo®, they were estimated through multiple stepwise regression models based on the detected body measures. The authors themselves recognized the appropriateness of incorporating into the system an automatic method of anthropometric parameters acquisition, such as body circumferences. Finally, XSensor®, a company experienced in pressure sensors, developed Reveal®, a mattress recommendation system that, based only on the information from the pressure images, gives some suggestions about the most suitable mattress for the user.

1.2 Contribution

Overcoming some of the limitations of the aforementioned works, in this paper we propose a novel system combining 3D RGB-depth data from Kinect and 2D pressure images from a pressure-sensitive bedsheet to extract anthropometric landmark points and key pressure points which, incorporated to a mathematical model based on clinical knowledge that calculates the user's morphotype, weight, and height, recommends the most suitable sleep system in an individualized unobtrusive way. The pressure sensor is placed over an intermediate-density mattress and the Kinect device at zenithal position facing the mattress, which capture the data of the user's body lying on the mattress in supine position. Therefore, our system is able to compute the body categorization with just one body pose, thus reducing the required time and improving the user experience.

Specifically, in this paper we want to focus on the integration of the automatic landmark points extraction and pressure image analysis with a clinical knowledge-based prescription model. We propose a novel method that combines RGB and depth information to segment human bodies lying on a bed. Next, we divide the body in different body parts using a 3D model-based system whose body part labels and joints are assigned after aligning the model to the segmented body. Landmark anthropometric points are extracted by intersecting two thin plates: one orthogonal to the body crossing each joint point and the segmented body hull, from where we extract the extreme points, and other orthogonal to the

plane of the mattress crossing it and the maximum distance point of the result of the first intersection. This way, the system is able to compute supine and lateral distances. Finally, such measures are fused with at-risk points extracted from pressure images to obtain the final sleep system prescription, which is computed using a calculation algorithm based on physiological, morphological, and anthropometric parameters.

The proposed system was evaluated on a sample of 200 subjects, showing high correlation among manual and automatic measures. We demonstrate the effectiveness of the whole system to perform body mass index and morphotype categorization, which are used alongside pressure information for sleep system recommendation. The performance of the latter is also evaluated. The system is currently being applied to customers in a store setting.

The remainder of this article is organized as follows. Section 2 describes the clinical knowledge-based model used in the bed design prescription system, which is presented in Sect. 3. Details of the automatic methodology for extraction of prescription variables are described in Sect. 4. The complete system is evaluated in Sect. 5. Finally, Sect. 6 concludes our work.

2 Clinical Basis

In order to create the clinical knowledge-based model, we first determined the need for an anthropometric analysis by categorizing the users in different basic morphotypes for the Spanish population (Canda and de Deportes 2012; Romero Collazos 2008; Benjumea 2001; de Sanidad y Consumo 2008) from height and thoracic-, abdominal- and hip-perimeter measures. An example of the morphotype categorization M_C is shown in Fig. 1. The Body Mass Index (BMI) BMI and its categorization BMI_C, which can be calculated from height and weight, were performed according to internationally given intervals. Adult BMI (kg/m^2), according to World Health Organization (WHO), is stratified in: *Underweight*<18.49, *Normal range* 18.5–24.99, *Overweight* 25–29.99, *Obese* 30– 39.99, and *Morbidly obese* $\geq$ 40 (Joint et al. 1985). Similarly, we used the recommended international intervals for children and people older than 65 years, according to the international organizations. The differences between genders give slightly different intervals for overweight and obese categories, but for the purpose of this study the differences do not provide any substantial change.

The mathematical equations used in the model were defined based on geometric formulas and formulas used in clinical medicine care (Determann et al. 2007). Weight W was estimated using Lorenz formula (2007), which is one of the most useful approximations for weight estimation by indirect means in a clinical setting, approximating

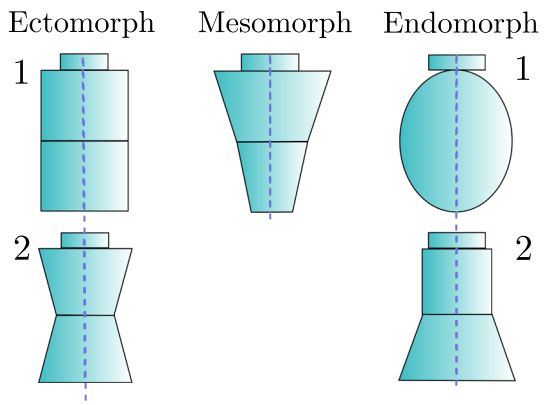

Fig. 1 Morphotype categorization

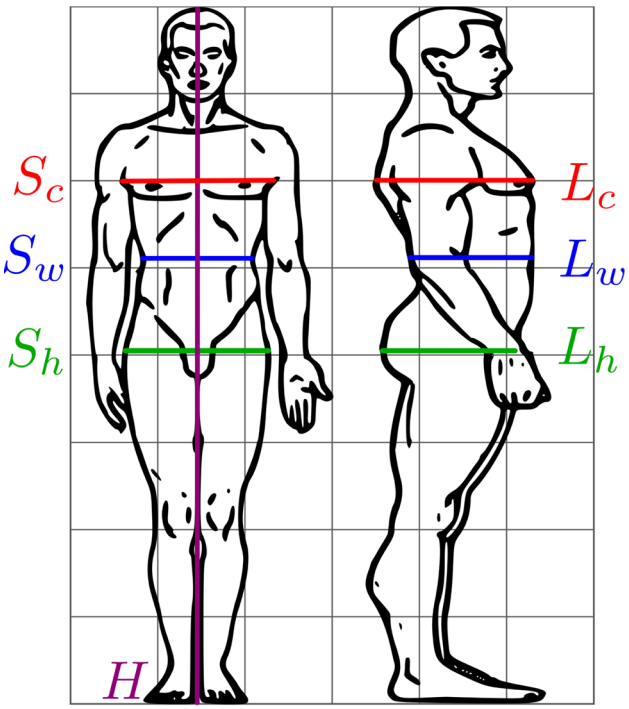

Fig. 2 Segments between anthropometric landmark points used in the general calculation algorithm

the body weight from anthropometric measures as simple as height, waist, and hip circumferences. We included the corrections that the numerical model suggested to improve accuracy. Chest, waist, and hip circumferences (C_c, C_w, and C_h, respectively) were estimated using the measures of lateral and supine maximum diameters of the chest zone (at nipple level), waist (at navel level), and hips (at trochanteric level). Such measures are represented in Fig. 2. Using them we modeled each body circumference as an ellipse, taking the supine diameter as the major axis, and the lateral diameter as the minor axis. In order to obtain the morphotype categorization M_C internationally recognized for Caucasians, we used the ratio between chest, waist, and hips, as shown in Fig. 1.

Based on the morphotype and BMI categorizations, we created a categorization matrix corresponding to the density of the mattress, giving a neutral density value (0, intermediate density, 3.3 Kpa) to people with *Mesomorph/Normal range*, *Ectomorph2/Overweight*, *Endomorph1/Overweight*, and *Endomorph2/Overweight* categories, as being those subjects who best fit their pressure distribution on the mattress surface. Four additional density values were also used in the categorization matrix, two for firmer mattresses (+1, +2) and two for softer ones (−1, −2), being the firm categories applied to BMI higher intervals and the soft categories to BMI lower intervals. Having such categorization, we could assign each density value to a different prescribed mattress R_M.

The aim of topper prescription R_T is to further individualize the sleep system prescription, categorizing each subject in a more precise way, based on the number of pressure points with a pressure value higher than 60 mmHg over the mattress surface – at-risk points. We decided this interval since pressure points with value higher than 60 mmHg may cause subcutaneous ischemia, forcing the subject to change his posture due to the discomfort caused by the excess of pressure. Then, if the sum of the mattress density value and the number of pressure points higher than 60 mmHg was less than 2 we prescribe the most rigid topper, if the sum was equal to 2 we prescribe the medium rigidity topper, and the soft one otherwise, in order to reduce the number of points greater than 60 mmHg and balance the distribution of body weight on the mattress surface as much as possible.

Regarding the pillow prescription R_P, we took as measuring point the point of maximum pressure on the surface of the occipital bone in supine position, considering that when the pressure exerted is between 30 and 40 mmHg, the pressure is adequate and therefore we prescribe a medium density pillow. For lower pressure values we prescribe a harder pillow, whereas a softer pillow is recommended for higher pressures. This way we ensure that the curvature of the cervical spine in supine position is the most appropriate for each person. The pressure exerted by the head in lateral position was not taken into account after observing empirically that it depends more on a correct pressure exerted by the shoulder on the mattress surfaces.

Finally, based on the aforementioned measures and objective pressure distribution data, we elaborated an index or categorization for sleep system design SSD, consisting of mattress, topper, and pillow individualized prescriptions. The final general calculation algorithm and the variables that determine the sleep system prescription are depicted in Fig. 3.

The validation of the model is crucial before establishing specific recommendations that may have clinical repercussion (Bain et al. 2003) and affect the users' perceived comfort. An analysis of 200 people (72 men, 128 women, average age 33.82 ± 23.02, from 4 to 93 years old) was conducted

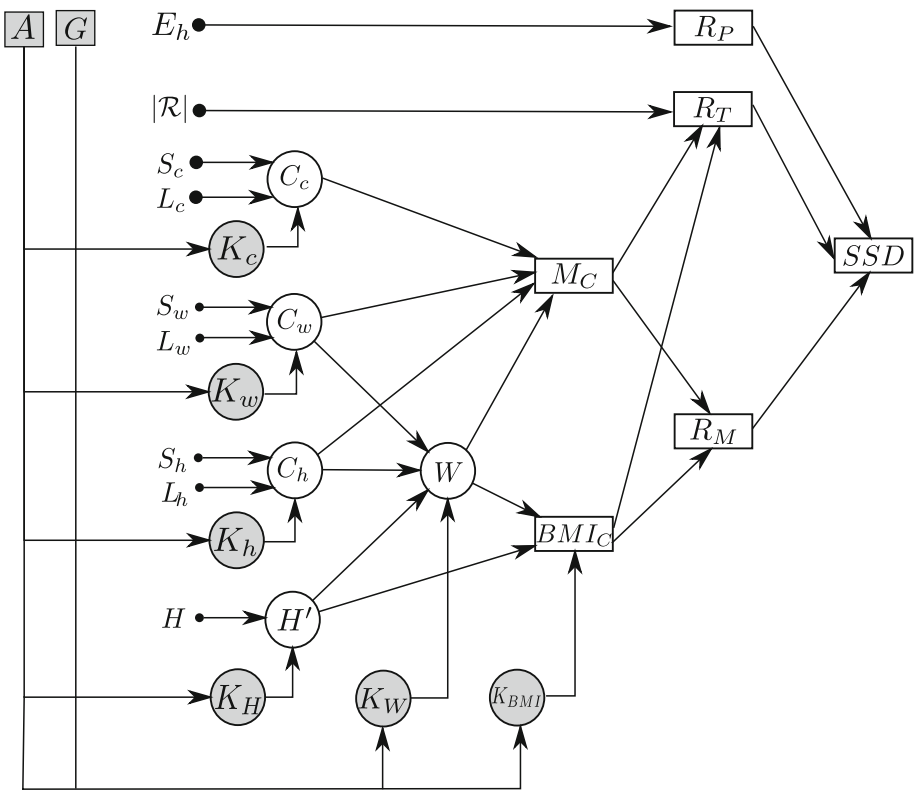

Fig. 3 General calculation algorithm and application of prescription variables. Isolated variables serve as input for the algorithm. *Circles* indicate numerical variables whereas *squares* indicate categorical ones. *Shaded* variables are observed

in order to validate the mathematical formulas of the sleep system predictive model. First, body circumferences, height and weight were manually measured with a measuring tape and an analog weighing scale. BMI and morphotype were calculated from the manual measures, which were taken as gold standard. Then, the set of prescription variables of the proposed model were also manually measured, that is, lateral and supine maximum diameters of chest, waist, and hip zones, and height. Body circumferences, weight, BMI and morphotype categorizations were derived from the mathematical model. The comparison of manual measures to the measures obtained by the proposed model achieved statistically significant results, thus validating the predictive power of the model.

Such results substantiated the aim of automating the whole process in a real application, using the clinical knowledge-based model with the needed variables extracted automatically in a non-contact manner, thus increasing the feasibility of the data acquisition methodology for a store setting. Furthermore, the mathematical model includes a set of correction factors for each of the variables (K_c, K_w, K_h, K_H, K_W, K_{BMI}). They are added to the mathematical formulas of the model, and are designed to increase the accuracy of its own prescriptions. Such factors could only be modified by contrast between the real data and automatic measures to further improve the model and the prescription accuracy using new subject samples, which can be thought of as a dynamic and smart personalized bed design prescription system. The proposed automatic system is presented in the following section.

3 System Overview

To facilitate the task of recommending a sleep system in a store setting, the data acquisition methodology of an automatic recommender system should be easy and intuitive for both customer and salesperson. It should be able to measure customer's anthropometric data without placing markers on the human body, in a non-contact manner and without requiring especial clothes. Furthermore, the computation of the measures and the output of the recommendation should be quick in order to guarantee customer satisfaction. In this section we present the characteristics of the system, which aims at satisfying the aforementioned conditions.

3.1 Sensors

The 3D data of the scene is acquired from Microsoft Kinect for Windows v2 device, which combines depth sensing technology, a built-in CMOS color camera sensor, an infrared (IR) emitter, and a microphone array. The depth sensor relies on Time-of-Flight technology, which captures 3D video data under any ambient light conditions with a practical range of 0.8–4 m. The device possesses a 70° horizontal and 60° vertical field of view. The color video stream comes at 1080p in YUY2 format, whereas the depth stream has a resolution of 512 × 424 pixels with 16-bit depth, which corresponds to the distance in millimeters at 1 mm accuracy; that is, the value of each pixel in a depth frame is the distance in mm of the corresponding surface part of the object from the sensor. Both streams work at 30 fps, although in poor lighting conditions the color stream decreases to 15 fps. Along with Kinect for Windows SDK 2.0, depth data can be projected and re-projected from 2D image space to 3D camera space, and allows RGB-depth mapping.

Additionally, pressure data is gathered from an in-house capacitive pressure-sensitive mattress sensor with a resolution of 26 × 64 sensing points and 31.75 mm pitch within its 81 × 203 cm sensing area. It has a measuring range of 5 to 100 mmHg and runs at a sampling rate of 53 Hz.

3.2 Setup

Figure 4 shows the scheme of our proposed setup. The pressure sensor is placed over an intermediate-density mattress, both covered by an especial monochromatic 3D mesh fabric that is adjusted to the mattress so as to avoid wrinkles—in our setup we use a black one, but it could be any. The Kinect device is located at zenith position facing the mattress at a minimum distance of 1.40 m. Both sensors are connected to the same computer, which runs the sleep system recommender application. We also use dedicated lighting above the mattress to ensure homogeneous illumination and avoid shadows. The homogeneous lighting and monochromatic background are meant to ease the body segmentation task. Note that the goal of the system is to be used in a store setting, so the illumination conditions are controlled; however, little RGB difference between the background and the

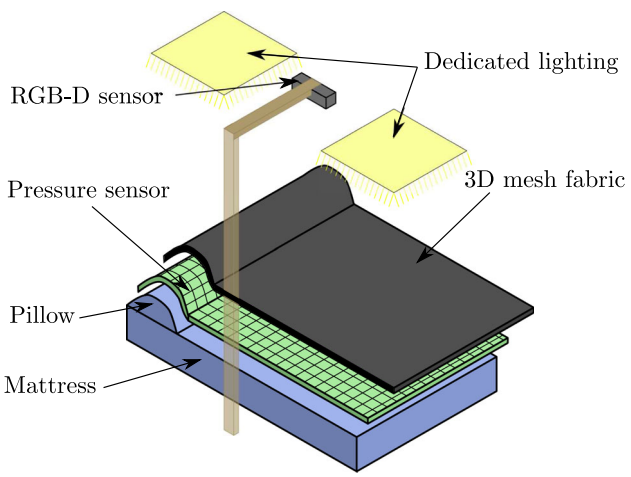

Fig. 4 Scheme of the proposed setup

Fig. 5 Real setup examples

person is needed to successfully segment the person. Two examples of real store setups are shown in Fig. 5.

3.3 Pipeline

Users are asked to lie over the mattress in supine position with arms separated from the body and legs slightly apart. Loose clothes should be tighten to the body and long hair should be pulled aside under the head, so as to provide a good definition of the body contour. A 3D point cloud of the scene with color information is captured, along with the pressure image from the pressure sensor. Both representations are analyzed separately.

In the first place, the human body and the plane of the mattress are segmented from the 3D scene. We then extract the anthropometric landmark points that can be seen from the supine position, which are the extreme points of chest, waist and hip body parts and measure their distance (S_c, S_w, and S_h, respectively). Height (H) is also obtained from such position. In order to extract lateral measures of the body, the distances from the highest point of thoracic, abdominal and hip body parts to the plane of the mattress are computed (L_c, L_w, and L_h, respectively).

In the second place, the pressure image is analyzed, from where we extract the number of at-risk points ($|\mathcal{R}|$) and the pressure exerted by the head (E_h).

The computed parameters are introduced to the clinical knowledge-based model, which calculates the body circumferences (C_c, C_w, and C_h), weight (W), BMI value (BMI) and categorization (BMI_C), and morphotype categorization (M_C), according to the gender (G) and age (A) of the user. Depending on the results, and taking also the pressure information into account, the system recommends the most suitable mattress-topper-pillow combination.

Figure 6 depicts the different stages of the system's pipeline. Next section describe the details of the proposed methodology for automatic body segmentation, body landmark points extraction and pressure image analysis.

4 Automatic Extraction of Prescription Variables

The RGB-D 3D point cloud data captured by Kinect contains the whole scene, that is, the human body but also the pillow and the mattress where the body lies, and maybe other artifacts. To further process the body for extracting the landmark points, the first step is to segment it from the rest of the scene. Since the obtained point cloud is organized, that is, structured in an image-like grid, let us denote it as a set of indexed 3D world coordinates with RGB information $\mathcal{P} = \{\mathbf{p_{i,j}} = (x, y, z, r, g, b) \mid \forall i \in \{1, \ldots, n\}, \forall j \in \{1, \ldots, m\}\}$, where the 2D indices i, j indicate the i and j locations of the point in the image-like grid structure. That means that the structure can be also represented as a 2D image where each pixel i, j has the RGB information associated to the point $\mathbf{p_{i,j}}$, denoted by $c_{i,j}$. n and m denote the width and height of the point cloud scene, respectively.

4.1 Human Body Segmentation in Supine Position

In order to extract the human body from the point cloud $\mathcal{P}$, isolated color-based subtraction or depth-based techniques

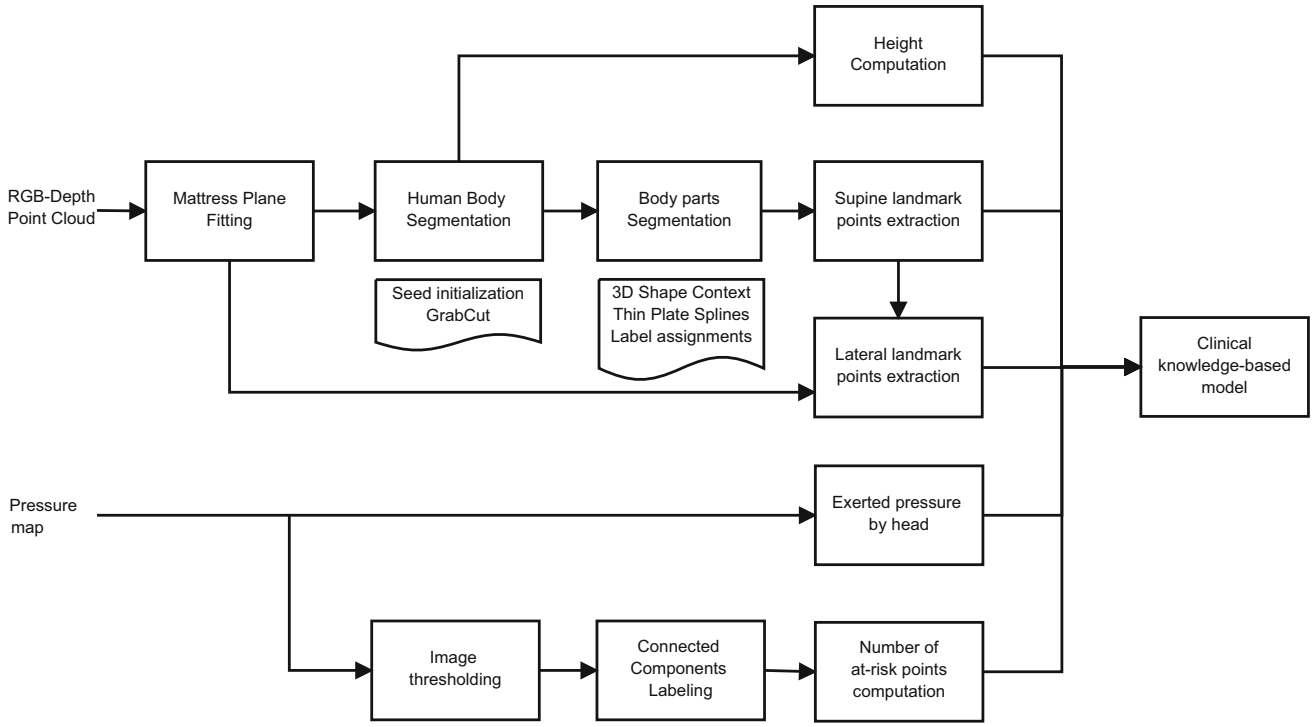

Fig. 6 Overall block diagram of the pipeline

are not enough due to the irregular surface of the mattress—which includes the pillow and possible wrinkles—, and similarities in the color distribution between the color of the mattress and the user's clothes. For that reason, we propose to combine both color and depth information with the iterative GrabCut algorithm (Rother et al. 2004) to refine the final segmentation. Given that the setup is fixed, with no changes in color background and lighting, we can learn a prior of the background color model, and also rely on depth information to extract a prior of the human body, and introduce such seeds into Grabcut. The procedure is explained below.

4.1.1 GrabCut Segmentation

GrabCut finds a binary segmentation—background and foreground—of an image by using Gaussian Mixture Models (GMMs) to specify the color distribution of background and foreground pixels. Given a color image I, a Gaussian mixture considers the array $\mathbf{c} = (c_1, \ldots, c_N)$ of N pixels where $c_n = (r_n, g_n, b_n)$:

$$p(\mathbf{c}|\mu_k, \Sigma_k, \pi_k) = \sum_{k=1}^{K} \pi_k p_k(\mathbf{c}), \pi_k \geq 0, \sum_{k=1}^{m} \pi_k = 1, \quad (1)$$

$$p_k(\mathbf{c}) = \varphi(\mathbf{c}|\mu_k, \Sigma_k) = \frac{1}{(2\pi)^{d/2}|S_k|^{1/2}} \exp\left\{ -\frac{1}{2}(\mathbf{c} - \mu_k)^T \Sigma_k^{-1}(\mathbf{c} - \mu_k) \right\}, \quad (2)$$

where K is the number of mixtures, $\mathbf{c}$ is the normal distribution density with mean μ_k and covariance matrix Σ_k, and π_k is the weight of the k-th mixture.

GrabCut method defines the segmentation result as an array $\alpha = (\alpha_1, \ldots, \alpha_N)$, where $\alpha_n \in \{0, 1\}$, assigning a label to each pixel of the image indicating if it corresponds to background or foreground, respectively. Initial labels are defined in a semi-automatic way as a quadmap $\mathcal{Q}$ that consists of: $\mathcal{Q}_\mathcal{B}$ set of definitive background pixels, $\mathcal{Q}_\mathcal{F}$ set of definitive foreground pixels, $\mathcal{Q}_{\mathcal{PF}}$ set of pixels that are probably foreground, and $\mathcal{Q}_{\mathcal{PB}}$ with probably background pixels. Pixels belonging to $\mathcal{Q}_\mathcal{B}$ and $\mathcal{Q}_\mathcal{F}$ are directly set as background and foreground, respectively, which means that GrabCut will not be able to modify their labels, whereas unknown labels ($\mathcal{Q}_{\mathcal{PB}}$ and $\mathcal{Q}_{\mathcal{PF}}$) are actually the ones the algorithm will treat.

A full covariance GMM of K components is defined for background pixels ($\mathcal{Q}_{\mathcal{PB}}$ and $\mathcal{Q}_\mathcal{B}$) and another for foreground pixels ($\mathcal{Q}_{\mathcal{PF}}$ and $\mathcal{Q}_\mathcal{F}$), parametrized as follows:

$$\theta = \{\pi(\alpha, k), \mu(\alpha, k), \Sigma(\alpha, k), \alpha \in \{0, 1\}, k{=}[1, \ldots, K]\}. \quad (3)$$

We also consider the array $\mathbf{k} = \{k_1, \ldots, k_N\}, k_n \in \{1, \ldots, K\}, n \in [1, \ldots, N]$, indicating the component of the background or foreground GMM the pixel c_n belongs to. The Gibbs energy for segmentation is then:

$$\mathbf{E}(\alpha, \mathbf{k}, \theta, \mathbf{c}) = \mathbf{U}(\alpha, \mathbf{k}, \theta, \mathbf{c}) + \mathbf{V}(\alpha, \mathbf{c}), \quad (4)$$

where $\mathbf{U}$ is the likelihood potential, based on the probability distributions $p(\cdot)$ of the GMM:

$$\mathbf{U}(\alpha, \mathbf{k}, \theta, \mathbf{c}) = -\log p(c_n|\alpha_n, k_n, \theta_n) - \log \pi(\alpha_n, k_n), \quad (5)$$

and $\mathbf{V}$ is a regularizing prior, penalizing color differences within the neighborhood $\mathbf{C}$ around each pixel:

$$\mathbf{V}(\alpha, \mathbf{c}) = \gamma \sum_{(m,n)\in\mathbf{C}} [\alpha_n \neq \alpha_m] \exp(-\beta \|c_m - c_n\|^2). \quad (6)$$

With the energy minimization scheme and given the initial quadmap $\mathcal{Q}$, the final segmentation is obtained by Graph Cuts min-cut algorithm (Boykov and Funka-Lea 2006).

4.1.2 Seeds Initialization

Our proposal is based on the previous framework. In order to increase the accuracy of the segmentation algorithm, we create seeds for each of the label regions exploiting spatial and appearance prior information to introduce them into GrabCut.

The point cloud pre-processing starts by filtering the point cloud $\mathcal{P}$ along the z dimension to discard possible elements over or under the setup location that may interfere with the following procedures. Therefore, a point is kept if its z component is within a given range t_1 and t_2, otherwise, it is set to NaN.

Then, we segment the mattress by fitting a plane model $ax + by + cz + d = 0$ from $\mathcal{P}$ using Random Sample Consensus (RANSAC) method (Fischler and Bolles 1981) to generate model hypotheses, as in Rusu (2013). We use a distance threshold d_t that determines the maximum distance allowed for a point to be part of the mattress plane. We define the obtained plane as $\lambda = (a, b, c, d)$. The set of points of the segmented mattress plane $\mathcal{P}_\mathcal{P} \in \mathcal{P}$ are considered as our first Background seed. To obtain a first Foreground seed, we take all the points over a certain distance d_p of the plane of the mattress, in such a way that we just take points that belong for sure to the human body—without taking the pillow into account, which we will consider later. We compute the point-to-plane distance as:

$$d_p = \frac{ax + by + cz + d}{\sqrt{a^2 + b^2 + c^2}}. \quad (7)$$

Up to this point, we have two initial seeds: one for Background containing samples of the mattress, but also possible human body parts such as parts of the hands, due to their shallow depth; and another for Foreground, which contain body samples but also part of the pillow. For that reason, such seeds have to be further refined so as to eventually obtain an accurate quadmap Q.

We start by refining the Background seed. As explained in Sect. 3.2, the system's setup uses a monochromatic fabric over mattress and pressure sensor, which allows us to use the color information to discard those regions that do not belong to the background. To do so, we compare the color samples of the current Background seed to a previously trained GMM φ of K_φ components—during the setup configuration stage, without anybody lying on the bed—with the color distribution of the fabric, defined as in Eqs. 1 and 2, whose parameters were estimated applying Expectation Maximization (EM) algorithm (Dempster et al. 1977). We use the PDF of the GMM to calculate the log-likelihood probability of each sample of the Background seed $l(c_{i,j})$. Therefore, we initialize $\mathcal{Q}_\mathcal{B} = \{\forall p_{i,j} \in \mathcal{P}_\mathcal{M} | l(c_{i,j}) \geq t_B\}$, being t_B a defined threshold. We also initialize $\mathcal{Q}_{\mathcal{PB}}$ with the rest of the samples.

Next, we refine the Foreground seed. In particular, we need to refine the region where the pillow is located, as it is the only conflict part. To do so, we just take the subset of samples of the upper part of the scene, where the pillow is located—about 1/6 of the scene—, and compare them again to φ. Pixels whose log-likelihood is over a defined threshold t_F are classified in the Q_{PB} set. For those over t_F, we classify the inner part of the resulting region as Q_F and the rest as Q_{PF}. That is, the central part of the head is marked as definite foreground, but not the rest, in order to avoid possible mistakes in the final segmentation.

Note that NaN points from $\mathcal{P}$ have not taken into account in the quadmap yet. To not interfere in the GrabCut segmentation, we set the color information of those points to the mean of the most important component of φ and include them in Q_B. Furthermore, the region between Q_B, that belongs to the mattress, and Q_F, which belongs to the person, is included in Q_{PF}, to further refine the contour of the human body.

4.1.3 Final Segmentation

Once the quadmap is initialized, we apply the iterative minimization algorithm shown in Eqs. 3–6. After convergence, we obtain a segmentation array $\alpha' = \{\alpha'_{i,j}, \forall i, j\}$, which we use to filter the scene to segment the human body. Such segmentation may contain artifacts, which we remove with morphological operators. Therefore, we define the segmented human body as $\mathcal{P}_\mathcal{B} = \{\mathbf{p_{i,j}} \in \mathcal{P} | \alpha'_{i,j} = 1\}$.

4.2 Human Body Parts Segmentation

Once we have a clean point cloud of the subject $\mathcal{P}_\mathcal{B}$, the next step is to segment it in different body parts and obtain the body part joints. To do so, we rely on the method presented by Madadi et al. (2015), a model-based approach where body-

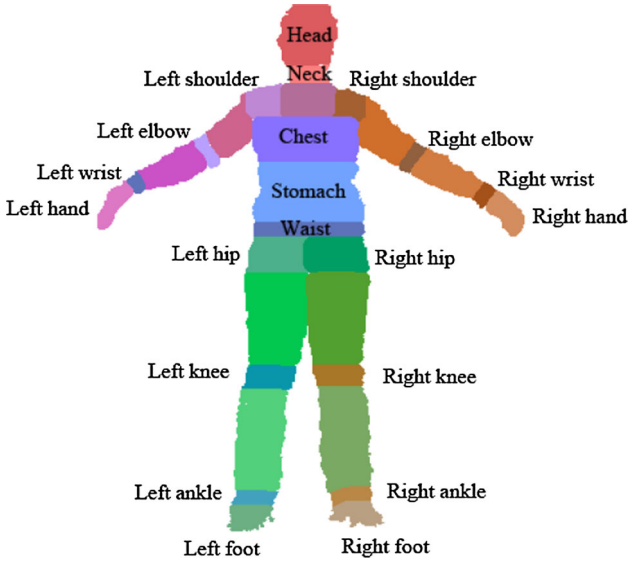

Fig. 7 Model with defined body parts (from Madadi et al. (2015)). Note that in our approach we compute the waist measure from the stomach segment

part labels of points are computed from a defined model after fitting a 3D shape context descriptor and subsequently aligning both point clouds. Since the subject pose in our system is restricted to supine position, we just use one frontal body model $\mathcal{P}_\mathcal{D}$ with 21 defined body parts, depicted in Fig. 7. In the following subsections we review the followed procedure.

4.2.1 Point Matching and Alignment

The first step is to find point correspondences between the model and the test subject. We employ the Shape Context descriptor of Belongie et al. (2002), which describes the coarse distribution of the rest of the shape with respect to a given point on the shape but extended to 3D data. The main idea of shape context is that, for a point $\mathbf{p_{i,j}}$ on the point cloud, a coarse histogram $h_{i,j}$ of the relative coordinates of the remaining $n-1$ is computed, such that:

$$h_{i,j}(k_b) = \#\{q \neq \mathbf{p_{i,j}} | (q - \mathbf{p_{i,j}}) \in \text{bin}(k_b)\}, \tag{8}$$

where k_b is the k-th bin of the histogram, being K_b the total number of bins, and q another point of the point cloud. As in Madadi et al. (2015), we use exponential space for the radius of nested spheres.

Therefore, we first downsample the point clouds to obtain a roughly-uniform spacing and then apply shape context. To find the best matching between all pairs of points described by shape context, we compute the matching cost based on the histogram and appearance similarity between each pair of points (p_i, q_i). The cost function is defined as:

$$C_{(p_i,q_i)} = \frac{1}{2}\Bigg[(1-\beta)\sum_{k_b=1}^{K_b}\frac{[h_i(k)-h_j(k)]^2}{h_i(k)-h_j(k)} + \beta(1-\cos(t_i - t_j))\Bigg], \tag{9}$$

where t_i and t_j denote the gradient angles at p_i and p_j, respectively. The function combines χ^2 test to find the histogram similarity cost, and the gradient angular difference polarity to find the appearance cost, which acts as a penalty function forcing smooth alignments on the surfaces, controlled by the smoothing coefficient β. We add redundant points to the matching process with a constant cost, so as to control the sensitivity of the descriptor to noise. The goal is to minimize the total cost of matching, which is considered a linear assignment problem that can be solved using Jonker and Volgenant (1987).

Next, we use the best point correspondences obtained to estimate an aligning transform using regularized thin-plate splines (Bookstein 1989), iteratively generating new coordinates and gradient angles to refine the alignment. Finally, the model is transformed to the test subject using the matching points. We refer the reader to the work of Madadi et al. (2015) for a detailed explanation of the transformation procedure.

4.2.2 Body Part Label Assignments and Joint Points

The new warped model, which contains the body part labels information, can be directly used to assign such labels to the test subject by point matching. We denote the assignment result as an array γ where $\gamma_{i,j} = [1, 21], \forall \mathbf{p_{i,j}} \in \mathcal{P}_\mathcal{B}$. The joint point of each part is defined as the center point of that part.

4.3 Landmark Points Extraction

After label assignment and joints extraction, the last step is to find the anthropometric landmark points needed for the clinical knowledge-based model. To do so, we use several geometrical approaches, which are explained below.

4.3.1 Supine and Lateral Measures

First, we define the principal axis of $\mathcal{P}_\mathcal{B}$ as the segment from the hip joint J_h to the neck joint J_n, denoted as $\overrightarrow{f_h f_n}$. Then, the orthogonal plane δ to $\overrightarrow{f_h f_n}$ can be estimated, so that the intersection of δ and $\mathcal{P}_\mathcal{B}$ in a given joint point f is o. Being p a point on the point cloud that belongs to o, p lies on δ plane if $\overrightarrow{op} \cdot \overrightarrow{of_h} = 0$ is fulfilled.

This way, we compute the orthogonal planes for chest, stomach and hip joints, and for each one we extract the extreme points that belong to the intersection, which are

the anthropometric landmark points for the supine position. Consequently, we compute the length of the line segments between the extreme points of each of those parts, obtaining S_c, S_w and S_h, respectively.

Finally, in order to extract the lateral measures for chest, stomach and hip parts, we find the point belonging to the intersection o that is at the maximum distance from the mattress plane λ computed previously. We compute such distance using Eq. 7. As a result, the maximum distance obtained for each of the parts is considered to be L_c, L_w and L_h, respectively.

4.3.2 Height Computation

In order to automatically compute the height of the human body point cloud $\mathcal{P}_B$, we compute the oriented bounding box (OBB) of $\mathcal{P}_B$ using Principal Component Analysis (PCA) and take its height as the height H of the body.

First of all, the covariance matrix and the mean position of the point cloud are computed in order to extract the eigenvectors (e_1, e_2, e_3) of the covariance matrix to compute the OBB. Secondly, a change of basis matrix T_h is built as:

$$T_h = \begin{pmatrix} r_x & u_x & t_x \\ r_y & u_y & t_y \\ r_z & u_z & t_z \end{pmatrix}, \quad \text{where } r = \frac{e_1}{||e_1||}, s = \frac{e_2}{||e_2||}, t = r \times s. \tag{10}$$

Then, each point in the point cloud $\mathcal{P}_B$ is transformed into the local frame of the OBB with the transformation matrix T^{-1} as follows:

$$p' = T^{-1} \cdot p, \forall p \in \mathcal{P}_M. \tag{11}$$

Finally, the minimum and maximum of each coordinate is found and stored into the points p'_{min} and p'_{max}, respectively. The height can be easily computed as:

$$H = p'_{max\,y} - p'_{min\,y}. \tag{12}$$

4.4 Pressure Image Analysis

Pressure map images I_p acquired by the pressure sensor have a resolution of 26×64 pressure points, where each point $e_i \in I_p$, $i = [1, \ldots, 26 \times 64]$ represents a pressure value in mmHg scale. As mentioned previously, the clinical knowledge-based model uses pressure imaging to extract the pressure exerted by the head and the absolute number of at-risk points, that is, points over a certain pressure threshold. The procedure to obtain such values is explained below.

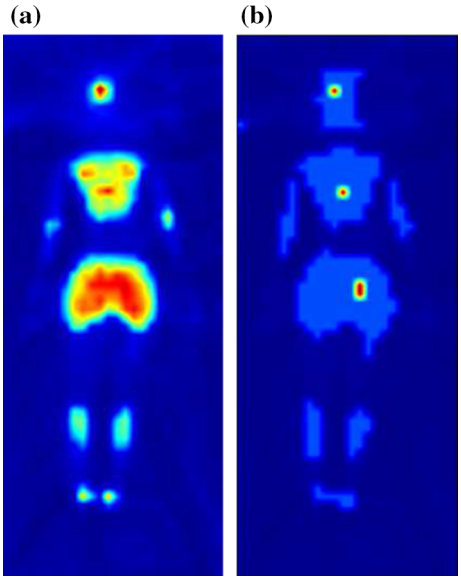

Fig. 8 **a** Original pressure image. **b** Thresholded image with at-risk points over 40 mmHg

4.4.1 Head Pressure

Due to the nature of the supine posture and our fixed setup, the subject's head is always located in the upper part of the image—about 1/6 of the pressure image—, denoted as I_{ph}. Therefore, we define the pressure exerted by the head as $E_h = \max_{i \in I_{ph}} e_i$.

4.4.2 Number of At-Risk Points

A thresholded pressure image shows connected regions of high pressure. Thus, a straightforward way to compute the number of at-risk points $|\mathcal{R}|$ is to apply connected components analysis (Suzuki et al. 2003) over that image. Let us define a thresholded image as ${I_p}^{(t_p)} = \{e_i \in I_p | e_i \geq t_p\}$ and its binary counterpart as $B({I_p}^{(t_p)})$. After labeling the resulting connected components in the binary image, we could just count them up. However, some connected components may contain more than one at-risk point, usually when the connected component is greater than a certain amount of pixels t_{ch}. In those cases, we iteratively increment t_p until the new connected components inside the original one have a dimension lower than t_{cl}. Once this refinement is done, the number of resulting connected components is considered as the number of at-risk points. An example of original and thresholded pressure map is shown in Fig. 8.

5 Evaluation and Validation

In order to present the results, we first describe the parameters and settings of the methods and the clinical knowledge-based

model validation procedure. Then, we present quantitative and qualitative results.

5.1 Parameters and Settings of Automatic Methods

The whole automatic approach is implemented in C++ using OpenCV and PCL libraries. For the human body segmentation part, we experimentally set $d_t = 2$ cm, $d_p = 4$ cm, $K_\varphi = 2$, $t_B = -18$, and $t_F = -30$ to maintain a trade-off between getting the maximum number of definite mattress and person samples while minimizing non-definite ones. Thresholds t_1 and t_2 of the pass-trough filter can be set manually while configuring the store setting, depending on the height from the RGB-D sensor to the mattress. For the multi-part body segmentation step, we keep the parameters of the original work of Madadi et al. (2015). The threshold used to get the number of at-risk points was set according to the clinical knowledge. Finally, the threshold parameters t_{ch} and t_{cl} can be modified by the user during the sleep system recommendation procedure in the store setting.

5.2 Final Model Validation

The set of 200 subjects that participated in the evaluation of the clinical knowledge-based model explained in Sect. 2 was also used to validate the mathematical model using the automatic methodology, and to determine the correction factors, which are added to the final mathematical model in order to adjust the parameters to improve accuracy. We used the measures obtained manually along with the quantity of at-risk points and pressure exerted by head determined by observation of the pressure images as gold standard. In addition, we computed the final prescription from the gold standard measures, which is used as the prescription ground truth.

In order to obtain the correction factors for each gender and age category, we adopted a leave-one-out strategy. For each fold, we determined the average deviations between the different real and automatic measurements of all the subjects except one, set such deviations as the correction factors and test the knowledge-based model along with the computed correction factors in the last subject. As metrics to validate the results, we use descriptive statistics for the segment distances and numeric variables. For BMI and morphotype categorization, we use the categorization accuracy. Furthermore, as BMI categorization is based on continuous numeric intervals, we propose an index using the level of displacement between BMI categories, defined as:

$$l_d = 1 - \frac{\sum_{i=1}^{N} \frac{displacement(i)}{\#categories-1}}{N}, \tag{13}$$

which represents the categorization accuracy based on the interval displacements, being N the number of subjects. Such measure could be applied to morphotype categorization. However, as the categorization is not based on continuous numeric intervals—it combines superior and inferior morphotype categories—, the result would not be representative.

Finally, to assess the performance of the whole system, we compare the final automatic prescriptions for mattress, topper, and pillow to the ground truth ones, both in terms of categorization accuracy and displacement accuracy.

5.3 Quantitative Anthropometric and Pressure Analysis Results

Table 1 summarizes the results obtained. As we can observe, the final model with the correction factors applied presents a margin of error ranging from 4.6 to 6.89 % in the determination of anthropometric variables—hip C_h, thoracic C_c, and abdominal C_w circumferences, and height H'—, and an average error of 10.1 % in weight W estimation.

People categorization into different morphotype intervals M_C presents a correlation of more than 80% with respect to reality, with a 71% of categorization accuracy. Fig. 9 depicts the classification accuracy. The confusion between manual *Endomorph 2* and automatic *Ectomorph 2* categories is due to their inferior morphotype similarity. A similar effect is noticed between *Endomorph 2* and automatic *Ectomorph 1*, which share similar superior morphotype. These similarities can be observed in Fig. 1.

Figure 10 shows the BMI_C categorization accuracy, where we obtain a coincidence up to 73.5 % and a displace-

Table 1 Descriptive statistics of the manual measures, automatic results, differences in mm and percentage error comparing manual and corrected automatic measures, and the Pearson correlation—significant at 0.01 level

Variable	Manual	Automatic	Error (mm)	% Error	Correlation
H'	161.20 ± 14.38	161.20 ± 16.21	-0.009 ± 84.86	0.21 ± 4.61	0.853
C_c	90.90 ± 12.18	90.90 ± 12.08	0.007 ± 60.97	0.23 ± 6.66	0.874
C_w	80.46 ± 13.48	80.46 ± 12.64	-0.001 ± 54.23	0.11 ± 6.89	0.916
C_h	97.73 ± 11.06	97.73 ± 10.56	-0.006 ± 59.19	0.15 ± 6.21	0.851
W	61.14 ± 15.66	61.68 ± 15.18	–	1.22 ± 21.68	0.899
BMI	23.19 ± 4.04	23.01 ± 4.39	–	2.68 ± 18.74	0.804

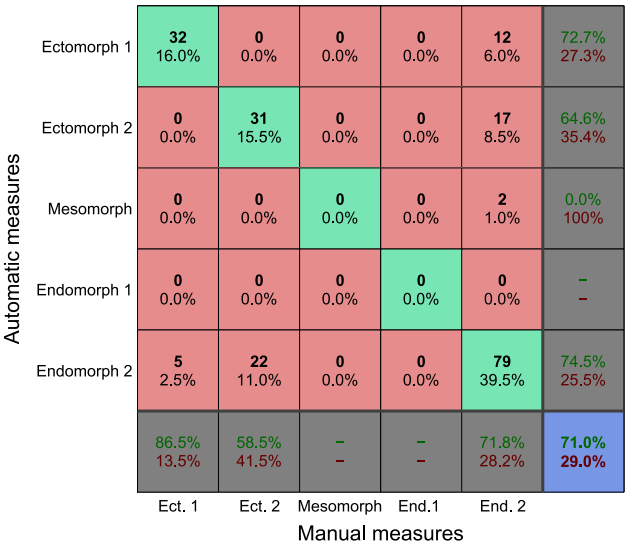

Fig. 9 Confusion matrix for Morphotype categorization

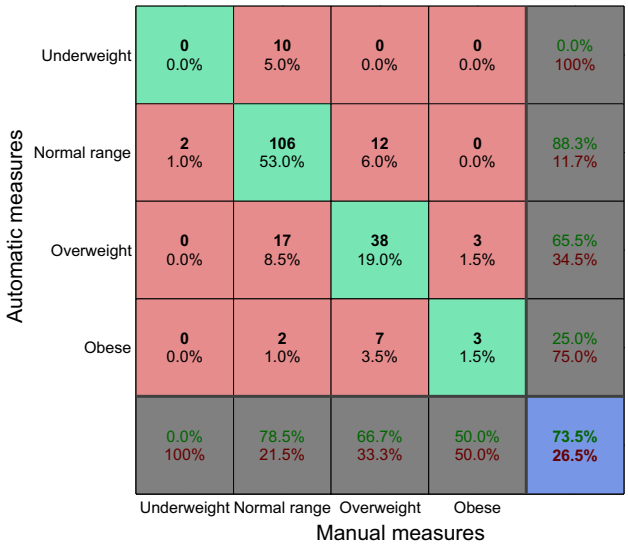

Fig. 10 Confusion Matrix for BMI Categorization

ment accuracy l_d of 91.27 %. It is worth noting that only two subjects where classified with a displacement of two categories.

Regarding the accuracy of the proposed solution for determining the number of at-risk points automatically, the straightforward comparison between the observed and automatically computed number reached a percent accuracy of 98.6 ± 0.5. The errors of the automatic procedure can be accounted for nearby points that may be considered as just one by the human annotator, and vice versa.

5.4 Quantitative Prescription Results

Automatic mattress prescription reached a categorization accuracy of 48.72 % and a displacement accuracy l_d of 85.9 %, showing that the displacement between categories is rather low. Automatic topper prescription obtained higher results, with 88.03 % of categorization accuracy and 93.5 % of displacement accuracy l_d. As the pillow prescription was straightforward only using the pressure exerted by the head, the accuracy obtained was 100%. These results support the usefulness and validity of the sleep system prescription application in a real store setting.

5.5 Qualitative Body Segmentation Results

Figure 11 shows some examples of human body and multi-parts segmentation, along with the automatic segment measures and the manual ones. The segmented body sometimes presents little parts of the background near the body contour, possibly due to the shadows cast by the body. However, we do not see a negative influence when performing multi-part body segmentation.

Indeed, multi-part segmentation errors may occur in the areas for which alignment is not perfect, mainly because of the effect of clothes. Furthermore, the similarity of the subject pose to the defined model plays an important role. The accuracy of measurements is directly related to the multi-part body segmentation accuracy. The neck segment plays a crucial role in determining the principal axis of the body, consequently affecting the correct extraction of landmark points.

When comparing the manual segments to the automatic ones, it is worth noting that the key element for the clinical knowledge-based model is their distance, even though their initial and ending points are not exactly the same. It is also interesting to mention that in some of the manual examples the chest segment C_h is marked slightly over the chest; however, the automatic procedure tends to mark it on the chest, where there is more distance in the z component. That is important to accurately extract the lateral measures. Note that the real measures were taken with measure tape, so the manual examples provided in Fig. 11 are just for comparison purposes.

Finally, we tested the system under low-light conditions, to assess its performance when there is no homogeneous illumination and shadows may be consequently present. As we can observe in Fig. 12, the segmented body contains little regions of background due to shadows casted by the human body. However, the resulting body circumferences are correctly computed, confirming that the system can still work properly in this setting, as little RGB difference is enough to perform the segmentation accurately.

Fig. 11 Qualitative results. *First column* shows the segmented human body. *Second column* depicts the segmented body parts along with the predicted body circumferences. *Third* and *fourth column* represent the computed and manual measures, respectively. Drawn segments represent the supine measures (S_c, S_h, and S_w), whereas *red circles* represent the points at maximum distance from the mattress plane, which are used to compute the lateral measures (L_c, L_h, and L_w)

Fig. 12 Test under low-light conditions. *First image* shows the complete scene. *Second image* depicts the segmented body. The *last image* represents the segmented body parts with the computed body circumferences

6 Conclusions and Future Work

We introduced a novel multi-modal RGB-Depth-Pressure system for sleep system recommendation that combines clinical knowledge along with automatic methods for extracting the needed variables in order to obtain the final prescription. In particular, we have proposed a novel method to segment human subjects lying on an irregular surface. Furthermore, we obtain the segmented body parts by applying 3D shape context descriptor to match the subject points to a defined model and align them using thin plate splines. Eventually, anthropometric landmark points are found applying an effective geometrical approach. We also computed pressure signal features from pressure information. Both qualitative and quantitative results demonstrate the predictive power of the model, with a correlation up to 80% with respect to reality. Therefore, the model is considered valid and reliable, containing the necessary mechanisms for self-improvement from new statistical data and from the increase in the size of included samples.

As future work, we plan to align pressure information—which can be considered as 3D—and the point cloud RGB-D data, in such a way that we obtain a complete body model with frontal and rear data. Therefore, we could also transfer multi-part body information to the pressure maps, in order to label possible at-risk points. Possible future improvements from a clinical point of view include: improving the prescriptive accuracy of the model, incorporating and prescribing additional technological improvements to the recommended sleep system, and applying the model to people with special needs, i.e. disabled people, athletes, people with physical conditions, etc.

Acknowledgments This work has been partially supported by Spanish Project TIN2013-43478-P and Dormity.com®.

References

Allen, B., Curless, B., & Popović, Z. (2004). Exploring the space of human body shapes: Data-driven synthesis under anthropometric control. Tech. rep., SAE Technical Paper

Azouz, Z. B., Shu, C., & Mantel, A. (2006). Automatic locating of anthropometric landmarks on 3d human models. In: *Third International Symposium on 3D Data Processing, Visualization, and Transmission*, pp. 750–757. IEEE.

Bain, D., Ferguson-Pell, M., & McLeod, A. (2003). Evaluation of mattresses using interface pressure mapping. *Journal of Wound Care*, *12*(6), 231–235.

Belongie, S., Malik, J., & Puzicha, J. (2002). Shape matching and object recognition using shape contexts. *IEEE Transactions on Pattern Analysis and Machine Intelligence*, *24*(4), 509–522.

Benjumea, A. C. (2001). Datos antropométricos de la población laboral española. *Prevención, trabajo y salud: Revista del Instituto Nacional de Seguridad e Higiene en el Trabajo*, *14*, 22–30.

Bookstein, F. L. (1989). Principal warps: Thin-plate splines and the decomposition of deformations. *IEEE Transactions on Pattern Analysis & Machine Intelligence*, *6*, 567–585.

Boykov, Y., & Funka-Lea, G. (2006). Graph cuts and efficient n-d image segmentation. *International Journal of Computer Vision*, *70*(2), 109–131.

Canda, A. S., & de Deportes, C. S. (2012). Variables antropométricas de la población deportista española. Consejo Superior de Deportes, Servicio de Documentación y Publicaciones.

Cippitelli, E., Gasparrini, S., Spinsante, S., & Gambi, E. (2015). Kinect as a tool for gait analysis: Validation of a real-time joint extraction algorithm working in side view. *Sensors*, *15*(1), 1417–1434.

Clarkson, S., Wheat, J., Heller, B., & Choppin, S. (2014). Assessing the suitability of the microsoft kinect for calculating person specific body segment parameters. In *Computer Vision-ECCV 2014 Workshops*, pp. 372–385. Springer.

de Sanidad y Consumo, M. (2008). Estudio antropométrico de la población femenina española.

Dempster, A. P., Laird, N. M., & Rubin, D. B. (1977). Maximum likelihood from incomplete data via the em algorithm. *Journal of the Royal Statistical Society Series B (Methodological)*, *39*, 1–38.

Determann, R. M., Wolthuis, E. K., Spronk, P. E., Kuiper, M. A., Korevaar, J. C., Vroom, M. B., et al. (2007). Reliability of height and weight estimates in patients acutely admitted to intensive care units. *Critical Care Nurse*, *27*(5), 48–55.

DeVocht, J. W., Wilder, D. G., Bandstra, E. R., & Spratt, K. F. (2006). Biomechanical evaluation of four different mattresses. *Applied Ergonomics*, *37*(3), 297–304.

Espitia-Contreras, A., Sanchez-Caiman, P., & Uribe-Quevedo, A. (2014). Development of a kinect-based anthropometric measurement application. In *2014 IEEE Virtual Reality (VR)*, pp. 71–72. IEEE.

Fischler, M. A., & Bolles, R. C. (1981). Random sample consensus: A paradigm for model fitting with applications to image analysis and automated cartography. *Communications of the ACM*, *24*(6), 381–395.

Foubert, N. (2010). Posture recognition and postural transition detection using bed-based pressure sensor. PhD thesis, Carleton University Ottawa.

Gordon, S. J., & Grimmer-Somers, K. (2011). Your pillow may not guarantee a good night's sleep or symptom-free waking. *Physiotherapy Canada*, *63*(2), 183–190.

Gordon, S. J., Grimmer-Somers, K., & Trott, P. (2009). Pillow use: The behaviour of cervical pain, sleep quality and pillow comfort in side sleepers. *Manual Therapy*, *14*(6), 671–678.

Gordon, S. J., Grimmer-Somers, K. A., & Trott, P. H. (2010). Pillow use: The behavior of cervical stiffness, headache and scapular/arm pain. *Journal of Pain Research*, *3*, 137.

Gupta, S., Markey, M. K., & Bovik, A. C. (2010). Anthropometric 3d face recognition. *International Journal of Computer Vision*, *90*(3), 331–349.

Harada, T., Mori, T., Nishida, Y., Yoshimi, T., & Sato, T. (1999). Body parts positions and posture estimation system based on pressure distribution image. In Proceedings of the 1999 IEEE international conference on robotics and automation (Vol. 2, pp. 968–975). IEEE.

Harada, T., Sato, T., & Mori, T. (2001). Pressure distribution image based human motion tracking system using skeleton and surface integration model. In *Proceedings 2001 ICRA IEEE international conference on robotics and automation* (Vol. 4, pp. 3201–3207). IEEE.

Huang, S. H., & Pan, Y. C. (2014). Ergonomic job rotation strategy based on an automated rgb-d anthropometric measuring system. *Journal of Manufacturing Systems*, *33*(4), 699–710.

Huang, W., Wai, A.A.P., Foo, S.F., Biswas, J., Hsia, C.C., & Liou, K. (2010). Multimodal sleeping posture classification. In *2010 20th international conference on pattern recognition (ICPR)*, pp. 4336–4339. IEEE.

Joint, F., Organization, W. H., et al. (1985). Energy and protein requirements: report of a joint fa.

Jonker, R., & Volgenant, A. (1987). A shortest augmenting path algorithm for dense and sparse linear assignment problems. *Computing*, *38*(4), 325–340.

Kim, H. S., Park, K. H., & Jeoung, J. W. (2013). Can we measure the intraocular pressure when the eyeball is against the pillow in the lateral decubitus position? *Acta Ophthalmologica*, *91*(7), e502–e505.

Lazzaro, E., Mallick, A., Singh, M., Reich, I., Elmann, S., Stefanov, D. G., et al. (2014). The effect of positional changes on intraocular pressure during sleep in patients with and without glaucoma. *Journal of Glaucoma*, *23*(5), 282–287.

Leilnahari, K., Fatouraee, N., Khodalotfi, M., Sadeghein, M. A., & Kashani, Y. A. (2011). Spine alignment in men during lateral sleep position: experimental study and modeling. *Biomedical Engineering Online*, *10*(1), 103.

Liu, J.J., Xu, W., Huang, M.C., Alshurafa, N., Sarrafzadeh, M., Raut, N., & Yadegar, B. (2013). A dense pressure sensitive bedsheet design for unobtrusive sleep posture monitoring. In *2013 IEEE international conference on pervasive computing and communications (PerCom)*, pp 207–215. IEEE.

Liu, J. J., Xu, W., Huang, M. C., Alshurafa, N., Sarrafzadeh, M., Raut, N., et al. (2014). Sleep posture analysis using a dense pressure sensitive bedsheet. *Pervasive and Mobile Computing*, *10*, 34–50.

López-Torres, M., Porcar, R., Solaz, J., & Romero, T. (2008). Objective firmness, average pressure and subjective perception in mattresses for the elderly. *Applied Ergonomics*, *39*(1), 123–130.

Lorenz, M. W., Graf, M., Henke, C., Hermans, M., Ziemann, U., Sitzer, M., et al. (2007). Anthropometric approximation of body weight in unresponsive stroke patients. *Journal of Neurology, Neurosurgery & Psychiatry*, *78*(12), 1331–1336.

Lorenzo-Navarro, J., Castrillón-Santana, M., & Hernández-Sosa, D. (2013). On the use of simple geometric descriptors provided by rgb-d sensors for re-identification. *Sensors*, *13*(7), 8222–8238.

Madadi, M., Escalera, S., Gonzalez, J., Roca, F. X., & Lumbreras, F. (2015). Multi-part body segmentation based on depth maps for soft biometry analysis. *Pattern Recognition Letters*, *56*, 14–21.

Martinez, M., & Stiefelhagen, R. (2014). Kinect unbiased. In *2014 IEEE International Conference on Image Processing (ICIP)*, pp. 5791–5795. IEEE.

Matsuo, J., Sugama, J., Sanada, H., Okuwa, M., Nakatani, T., Konya, C., et al. (2011). Development and validity of a new model for assessing pressure redistribution properties of support surfaces. *Journal of Tissue Viability*, *20*(2), 55–66.

Metsis, V., Kosmopoulos, D., Athitsos, V., & Makedon, F. (2014). Non-invasive analysis of sleep patterns via multimodal sensor input. *Personal and Ubiquitous Computing*, *18*(1), 19–26.

Miller, S., Parker, M., Blasiole, N., Beinlich, N., & Fulton, J. (2013). A prospective, in vivo evaluation of two pressure-redistribution surfaces in healthy volunteers using pressure mapping as a quality control instrument. *Ostomy/Wound Management*, *59*(2), 44–48.

Mogelmose, A., Bahnsen, C., Moeslund, T.B., Clapés, A., & Escalera, S. (2013). Tri-modal person re-identification with rgb, depth and thermal features. In *2013 IEEE conference on computer vision and pattern recognition workshops (CVPRW)*, pp 301–307. IEEE.

Nechala, P., Mahoney, J., & Farkas, L. G. (1999). Digital two-dimensional photogrammetry: A comparison of three techniques of obtaining digital photographs. *Plastic and Reconstructive Surgery*, *103*(7), 1819–1825.

Nguyen, T. V., Feng, J., & Yan, S. (2014). Seeing human weight from a single rgb-d image. *Journal of Computer Science and Technology*, *29*(5), 777–784.

Reyes, M., Clapés, A., Ramírez, J., Revilla, J. R., & Escalera, S. (2013). Automatic digital biometry analysis based on depth maps. *Computers in Industry*, *64*(9), 1316–1325.

Romero Collazos, J. (2008). Análisis de la forma y la proporcionalidad. antropometria aplicada a la nutrición.

Rother, C., Kolmogorov, V., & Blake, A. (2004). Grabcut: Interactive foreground extraction using iterated graph cuts. *ACM Transactions on Graphics (TOG)*, *23*(3), 309–314.

Rusu, R. B. (2013). *Semantic 3D object maps for everyday robot manipulation* (Vol. 85). Heidelberg: Springer.

Sáenz, Z. L., Arias, A., Guzmán, E. C., & Arias, d L. (2011). Analysis of ergonomics conditions of a brand of mattress and pillows. University-industry project, medellin-colombia. *Work (Reading, Mass)*, *41*, 1281–1287.

Suzuki, K., Horiba, I., & Sugie, N. (2003). Linear-time connected-component labeling based on sequential local operations. *Computer Vision and Image Understanding*, *89*(1), 1–23.

Uhm, T., Park, H., & Park, J. I. (2015). Fully vision-based automatic human body measurement system for apparel application. *Measurement*, *61*, 169–179.

Verhaert, V., Druyts, H., Van Deun, D., Berckmans, D., Verbraecken, J., Vandekerckhove, M., Haex, B., & Vander Sloten, J. (2011a). The use of a generic human model to personalize bed design. In: *Proceedings of 1st international symposium on digital human modeling*, vol 2202. Lyon, June, paper ID.

Verhaert, V., Druyts, H., Van Deun, D., De Wilde, T., Van Brussel, K., Haex, B., et al. (2011b). Modeling human-bed interaction: The predictive value of anthropometric models in choosing the correct bed support. *Work (Reading, Mass)*, *41*, 2268–2273.

Verhaert, V., Haex, B., Wilde, T. D., Berckmans, D., Verbraecken, J., Valck, Ed, et al. (2011c). Ergonomics in bed design: the effect of spinal alignment on sleep parameters. *Ergonomics*, *54*(2), 169–178.

Wang, Q., Jagadeesh, V., Ressler, B., & Piramuthu, R. (2014). Im2fit: Fast 3d model fitting and anthropometrics using single consumer depth camera and synthetic data. arXiv:1410.0745.

Wong, M., Lai, A., Singh, M., & Chew, P. (2013). Sleeping posture and intraocular pressure. *Singapore Medical Journal*, *54*(3), 146–148.

Yang, C., Mao, Y., Cheung, G., Stankovic, V., & Chan, K. L. (2014). Graph-based depth video denoising and event detection for sleep monitoring. In *2014 IEEE 16th international workshop on multimedia signal processing (MMSP)*, IEEE, pp 1–6.

Yousefi, R., Ostadabbas, S., Faezipour, M., Nourani, M., Tamil, L., & Pompeo, M. (2011). Posture and limb detection for pressure ulcer prevention. In *Proceedings of the Southern Biomedical Engineering Conference* (SBEC).

Yu, M. C., Wu, H., Liou, J. L., Lee, M. S., & Hung, Y. P. (2012). Breath and position monitoring during sleeping with a depth camera. In HEALTHINF, pp 12–22.

Zuberi, N. A., Rekab, K., & Nguyen, H. V. (2004). Sleep apnea avoidance pillow effects on obstructive sleep apnea syndrome and snoring. *Sleep and Breathing*, *8*(4), 201–207.